Available online at www.sciencedirect.com
ScienceDirect
Solid State Communications 144 (2007) 300–304
solid state communications
www.elsevier.com/locate/ssc

The effect of Ga doping in $Nd_{0.7}Sr_{0.3}MnO_3$ system

Yue Ying[a], Jiyu Fan[a], Li Pi[b,*], Bo Hong[a], Shun Tan[a], Yuheng Zhang[a,*,1]

[a] National High Magnetic Field Laboratory, University of Science and Technology of China, Hefei 230026, People's Republic of China
[b] Hefei National Laboratory for Physical Sciences at the Microscale, University of Science and Technology of China, Hefei 230026, People's Republic of China

Received 7 March 2007; received in revised form 2 August 2007; accepted 6 September 2007 by D.J. Lockwood
Available online 11 September 2007

Abstract

The structural, magnetic, and transport properties of the polycrystalline-doped systems $Nd_{0.7}Sr_{0.3}Mn_{1-x}Ga_xO_3$ ($0 \le x \le 0.20$) were investigated. For the parent and low-doped samples ($0 \le x \le 0.11$), they show a long-range ferromagnetic state below T_C and the Griffiths singularity above T_C. When x further exceeds 0.12, a transition from the metal ferromagnetic to the insulating cluster-spin-glass state as a function of Ga doping takes places at low temperatures. $x = 0.12$ is just a critical point x_c transforming from the Griffiths singularity to the cluster-spin-glass state.

PACS: 75.47.Lx; 72.15.Rn; 71.30.+h

Keywords: A. Cluster-spin-glass; A. Manganites; D. Doping; E. Griffiths singularity

1. Introduction

Manganites have been widely studied over the past decade years due to their exotic electrical and magnetic properties such as colossal magnetoresistance (CMR), charge ordering, orbital ordering, and phase separation [1–3]. It owes to the existence of the competitive interactions of double exchange (DE), antiferromagnetic superexchange, Jahn–Teller distortion and disorder in the manganites [3]. Recently, many investigations were carried on the effect of the elemental substitution on the Mn site. Generally, the substitution of most elements for Mn ions suppresses the Curie temperature T_C and the insulating–metal (I–M) transition temperature T_{IM} [4–8]. These effects mostly are referred to impurity effect, but the microscopic mechanism needs to be further investigated. Additionally, the Griffiths singularity in the manganites attracts interests recently. $La_{0.7}Ca_{0.3}MnO_3$ [9] and $La_{1-z}Sr_zMnO_3$ system [10] were investigated respectively. Griffiths [11] first considered a percolation-like problem in the diluted magnet in which each exchange interaction has value J_1 with probability p and $J_2 = 0$ with probability $1 - p$. The singularities arise in the temperature range ($T_C \le T \le T_G$) between the random transition T_C and the "pure" transition temperature T_G [10]. Bray et al. extended the argument to the system $0 \le J_2 < J_1$ where J_2 is the exchange interaction that reduces the transition temperature [12,13]. They termed the phase in the regime between T_C and T_G the "Griffiths phase". In $La_{0.7}Ca_{0.3}MnO_3$, Griffiths singularity is linked to CMR [9]. In the $La_{1-z}Sr_zMnO_3$ ($0.07 \le z \le 0.16$) system [10], the Griffiths singularity arising from the quenched disorder, which is due to the A site's doping, was reported.

In the above research [10], the Griffiths singularity takes place in the underdoped region, in which the number of Mn^{4+} is too few to generate long-range ordering. In this paper, we attempted to generate arbitrarily the short-range FM by Ga doping at B site in $Nd_{0.7}Sr_{0.3}MnO_3$ system, which exhibits the long-range FM order, to study the Griffiths singularity. The reason for choosing Ga doping is that the ionic radius of Ga^{3+} is close to that of Mn^{3+}, so its doping would not change the structure. Furthermore, Ga^{3+} is a nonmagnetic ion and the interaction between Ga and Mn ions could not take place. The structural, magnetic and transport properties of polycrystalline $Nd_{0.7}Sr_{0.3}Mn_{1-x}Ga_xO_3$ ($0 \le x \le 0.20$) were investigated. For the parent and low-doped samples ($0 \le x \le 0.11$), the Griffiths

* Corresponding author.
E-mail addresses: pili@ustc.edu.cn (L. Pi), zhangyh@ustc.edu.cn (Y. Zhang).
[1] Tel.: +86 551 3602808; fax: +86 551 3602808.

0038-1098/$ - see front matter © 2007 Elsevier Ltd. All rights reserved.
doi:10.1016/j.ssc.2007.09.002

singularity is found in $Nd_{0.7}Sr_{0.3}Mn_{1-x}Ga_xO_3$ system. For the high-doped samples ($x > 0.12$), the system appears as a cluster-spin-glass state.

2. Experiments

Polycrystalline $Nd_{0.7}Sr_{0.3}Mn_{1-x}Ga_xO_3$ ($0 \leq x \leq 0.20$) perovskite samples were synthesized with the conventional solid-state reaction method. Stoichiometric proportion of Nd_2O_3, $SrCO_3$, Ga_2O_3 and MnO_2 were mixed and first fired at 1000 °C for 24 h. Then they were repeatedly ground and heated at 1350 °C for 24 h to obtain better crystallization. Finally, the samples were pressed into pellets and sintered at 1350 °C for 24 h. The structure and phase purity has been checked by X-ray diffraction (XRD). The XRD analysis was carried out by a Rigaku-D/max-γA diffractometer using high-intensity Cu Kα radiation at room temperature. Resistivity measurements were performed by the conventional four-probe method in the temperature regime between 20 and 300 K. The magnetic properties were measured by a Superconducting Quantum Interference Device (SQUID) MPMS system. The measurements of the infrared (IR) transmission spectra (Nicolet 700) are carried out with powder samples in which KBr is used as a carrier. The IR spectra were collected in the frequency range from 350 to 4000 cm^{-1}. Raman scattering spectra were obtained on a Spex-1403 Raman spectrophotometer using a back-scattering technique.

3. Results and discussion

3.1. Structure

XRD patterns reveal that all the samples are single phase with Pbnm orthorhombic structure at room temperature, as shown in Fig. 1. In order to further explore the Ga-doping effect on the structure of the manganites, the IR and Raman spectra measurement were employed. The IR spectra are present in Fig. 2. Two absorption peaks appear at around 600 and 392 cm^{-1}, which correspond to the stretching mode υ_3 and bending mode υ_4 of MnO_6 octahedrons respectively. The mode υ_3 and υ_4 are sensitive to the bond length and the bond angle of Mn–O, respectively. Fig. 2 shows that the wave numbers of both the υ_3 and υ_4 almost have no change with doping, which exhibit that the substitution of Ga on Mn site does not change the vibrating spectra of system.

In the Raman spectra (Fig. 3), four scattering peaks appear at the frequency of around 244, 492, 613, and 710 cm^{-1}. For the 244 cm^{-1} peak, its frequency and intensity almost do not change with the increase in the doping level. For the 492, 613, and 710 cm^{-1} peak, their frequency almost does not change while their intensity strengthens with the increase in the doping level. XRD spectra exhibit that all samples show Pbnm orthorhombic structures, which is the same as those of $LaMnO_3$ and $PrMnO_3$ [14]. The site of 244, 492, and 613 cm^{-1} peaks is in agreement with that in $LaMnO_3$ and $PrMnO_3$. Therefore, the symmetry of 244 and 492 cm^{-1} peaks are assigned to be (in the Pbnm setting) A_g and the symmetry of 613 cm^{-1} is assigned to be B_{1g} [14,15]. The unchange of the frequencies

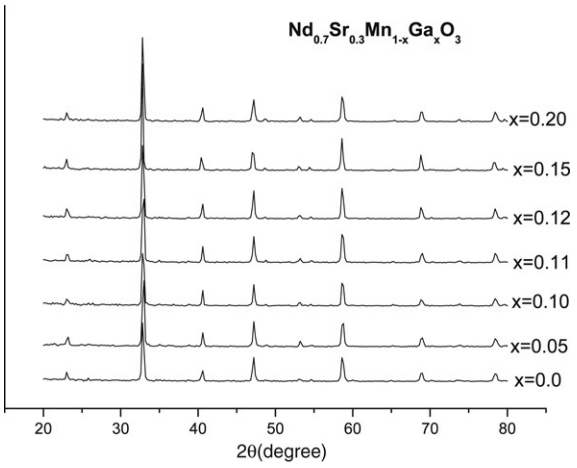

Fig. 1. X-ray diffraction patterns of the samples $Nd_{0.7}Sr_{0.3}Mn_{1-x}Ga_xO_3$ ($0 \leq x \leq 0.20$) at room temperature.

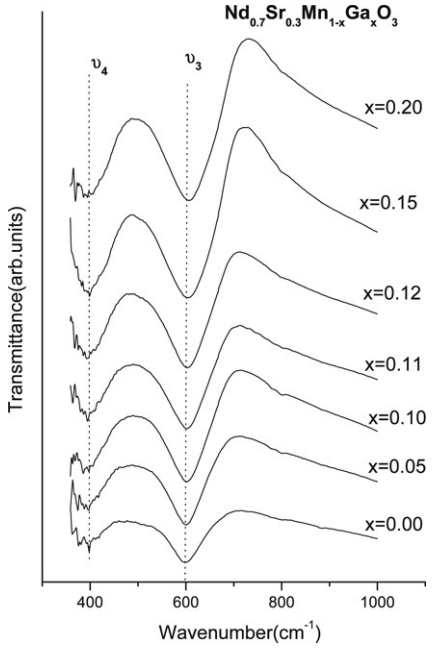

Fig. 2. Infrared transmission spectra of the samples $Nd_{0.7}Sr_{0.3}Mn_{1-x}Ga_xO_3$ ($0 \leq x \leq 0.20$) at room temperature.

of these three peaks exhibits the unchange of the structure, which consists with the result of IR spectra. It is known that the peaks at around 492 and 613 cm^{-1} correspond to the Jahn–Teller type mode and breathing mode in MnO_2 plane respectively [14]. For the 492 cm^{-1} peak in the parent sample ($x = 0$), because the itineration of e_g electron weakens the systemic Jahn–Teller effect, the Jahn–Teller mode is weaker. With the increase in x, the substitution of Ga^{3+} ions decreases the number of Mn^{3+}, which will weaken the Jahn–Teller mode. On the other hand, the substitution of Ga ion make that the e_g electron on Mn^{3+} is localized, which will be discussed in the following, so it will enhance the systematic intensity of the Jahn–Teller mode. The interaction of these two effects together results in the strengthening of the 492 cm^{-1} peak's intensity. As for the breathing mode which is competitive

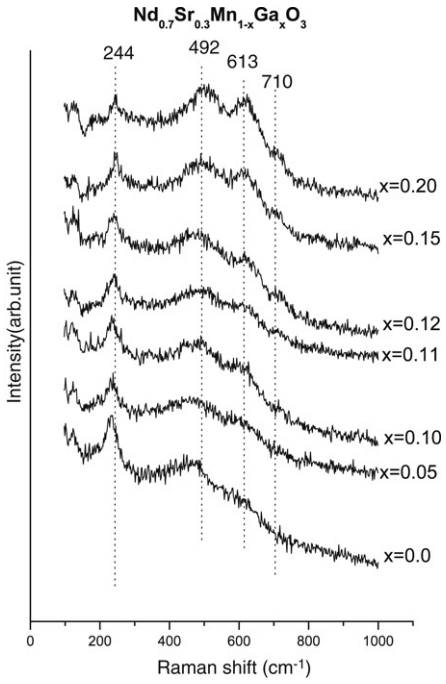

Fig. 3. Raman spectra of the samples $Nd_{0.7}Sr_{0.3}Mn_{1-x}Ga_xO_3$ ($0 \le x \le 0.20$) at room temperature.

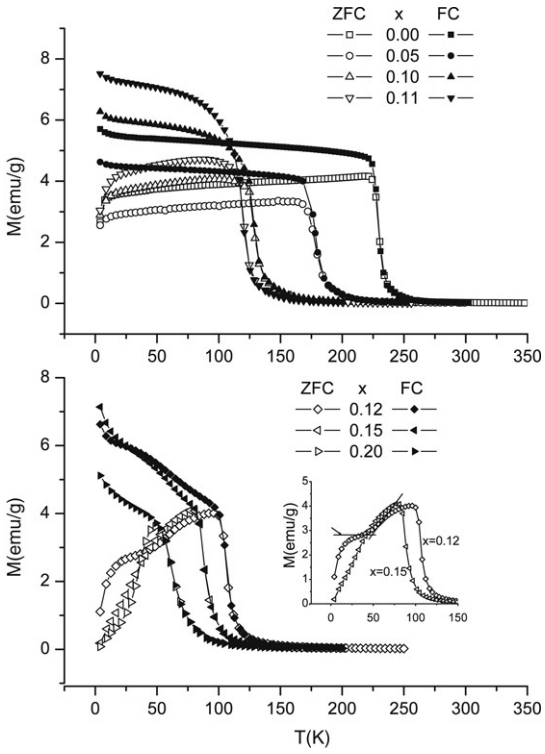

Fig. 4. Temperature dependence of magnetization in a 100 Oe magnetic field for $Nd_{0.7}Sr_{0.3}Mn_{1-x}Ga_xO_3$ ($0 \le x \le 0.20$).

with the Jahn–Teller mode, the increasing localization of e_g electrons will enhance the Jahn–Teller distortion and suppress the breathing mode of the oxygen ions around Mn^{3+} with increasing Ga concentration. Nevertheless, since the Ga^{3+} ion is a non-Jahn–Teller ion, the breathing mode of the oxygen ions around Ga^{3+} is strengthened with the increasing x.Thus the intensity of 613 cm^{-1} peak enhances remarkably. The new weak peak at 710 cm^{-1} could originate from the small distortion introduced by the Ga doping.

3.2. Magnetic and transport property

Fig. 4 shows the temperature dependence of magnetization $M(T)$ under zero-field-cooling (ZFC) process and field-cooling (FC) process at 0.01 T field for $Nd_{0.7}Sr_{0.3}Mn_{1-x}Ga_xO_3$ ($0 \le x \le 0.20$). The $M(T)$ curves of the parent and low-doped samples ($x \le 0.11$) exhibit a paramagnetic–ferromagnetic (PM–FM) transition. Their Curie temperature T_C, which is defined as the inflection point of the $M(T)$ curve, are listed in Table 1. It is obvious that T_C decreases with the increase in the doping level, which indicates that the DE interaction is suppressed by the Ga substitution. We can see two different kinds of $M(T)$ curves under ZFC in the figure. For the parent and low-doped samples ($x \le 0.11$), in the ZFC process, the magnetization is very strong at low temperatures and the curve is very flat instead of the drop with the decrease in temperature below T_C (Fig. 4(a)), which indicates that the long-range FM ordering forms in the parent and low-doped samples. When the doping level exceeds 0.12, the curves under ZFC drop quickly below T_C and the ZFC and FC curves appear as the "λ" shapes (Fig. 4(b)), which is the character of a cluster-glass state (CGS) [16]. Their transitional temperatures T_C are listed in Table 1. For $x = 0.12$ (shown in the inset of Fig. 4), with the decrease in temperature, the magnetization below T_C decreases firstly as one for $x = 0.15$, and then decreases slowly and flatly as one for $x = 0.11$.

Table 1
The PM–FM transition temperature T_C, I–M transition temperature T_{IM}, Griffiths temperature T_G and the deviation temperature T_D (see the text) for $Nd_{0.7}Sr_{0.3}Mn_{1-x}Ga_xO_3$ ($0 \le x \le 0.20$)

Sample (x) (K)	0.00	0.05	0.10	0.11	0.12	0.15	0.20
T_C	230.5	179.9	129.5	120.5	104.7	88.7	60.8
T_{IM}	231.4	180.2	130.5	121.3	98.4	–	–
T_G	261.8	228.9	192.9	192.9	–	–	–
T_D	250.6	243.9	242.1	237.0	–	–	–

We further investigated the transport property of the system and also found two kinds of resistivity curves which show very different behavior. The temperature dependence of the resistivity ($\rho(T)$) is shown in Fig. 5. For the samples with $0 \le x \le 0.11$, the curves undergo an insulating–metal transition. The transition temperatures T_{IM}, defined as the maximum point of the $\rho(T)$ curve, is listed in Table 1. T_{IM} is accordant with the corresponding T_C well. When the doping level exceeds 0.12, the curves show insulating behavior in the whole detecting temperature region. For the samples with $x = 0.15$ and 0.20, the resistances at low temperatures ($T < 50$ K) are so large that the values excess the measurement range of instrument and have not been recorded. We checked the resistances at 4.2 K for these two samples and they are too large to be measured, which implies that no insulating–metal transition takes place at low temperature region for these two samples.

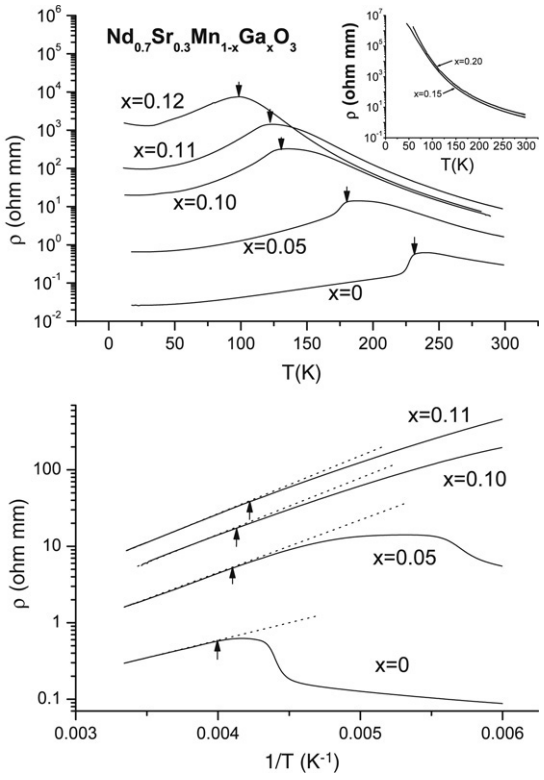

Fig. 5. Temperature dependence of resistivity for $Nd_{0.7}Sr_{0.3}Mn_{1-x}Ga_xO_3$ ($0 \leq x \leq 0.20$). The lower panel shows the relationship between the resistance and the inverse temperature for low-doped samples ($x \leq 0.11$).

However, the magnetic measurement shows that they exhibit FM in the low temperature region. The insulating behavior takes place in the FM region. For $x = 0.12$, it undergoes an insulating–metal transition as the samples with $x \leq 0.11$. According to the Table 1, for $x \leq 0.11$, T_{IM} is slightly larger than the corresponding T_C (~1 K), but for $x = 0.12$, T_{IM} is much lower than T_C (~6 K). It is apparent that $x = 0.12$ is a critical point.

3.3. Discussions

We further investigated the temperature dependence of the inverse magnetization ($M^{-1}(T)$) for the samples with $x = 0$, shown in Fig. 6. For the parent sample ($x = 0$), the $M^{-1}(T)$ curve shows a sharp downturn above Curie temperature T_C, which indicates the occurrence of FM phase. Griffiths pointed out that the short-range FM phases are formed above T_C. Generally, it is identified as the Griffiths singularity [17]. The Griffiths temperature T_G, which is defined as the onset temperature of this sharp downturn, is 261.8 K. The Griffiths phase occurs in the temperature region between T_G and T_C. In the Griffiths phase, there is no interaction between the short-range FM clusters, which means that these clusters are separate and disordered. Thus they make little contribution to magnetization. When temperature decreases below T_C, the interaction between these short-range clusters takes place, and then the long-range FM order forms, which results in a PM–FM transition-like in the $M(T)$ curve under ZFC. When the temperature decreases below T_G, the system begins to

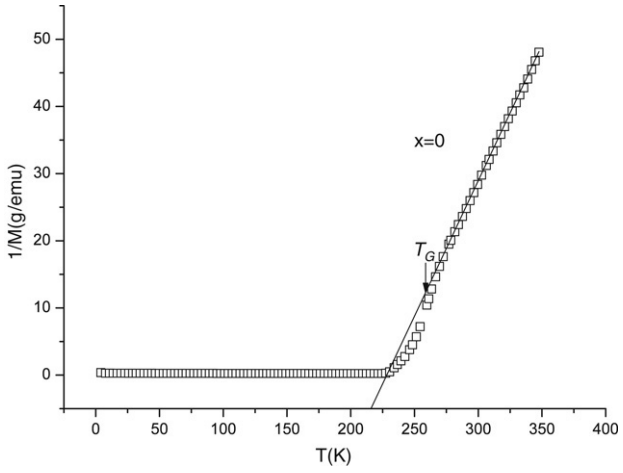

Fig. 6. Temperature dependence of the inverse magnetization in a 100 Oe magnetic field for $Nd_{0.7}Sr_{0.3}MnO_3$ ($x = 0$).

enter Griffiths phase with short-range FM ordering. When the temperature further decreases to T_C, the interaction between these small short-range FM phase promotes the formation of the long-range FM ordering in the whole system. For the low-doped samples with $0.05 \leq x \leq 0.11$, their $M^{-1}(T)$ curves show the similar behavior as $x = 0$ and their T_G is listed in Table 1. We also check the $\rho(T)$ curves in Fig. 5. It can be seen that the temperature at which the $\rho(T)$ curve deviates from the insulating behavior is not accurately coincident with T_{IM} or T_C, but obviously higher than T_{IM}. To see it more clearly, we plotted the relationship between the resistivity and the inverse temperature $\rho(T^{-1})$ for the low-doped samples ($x \leq 0.11$), shown in the lower panel of Fig. 5. For the $x = 0$ sample, the deviation from the insulating behavior is obvious at around 250.6 K, which is well above T_{IM} or T_C. For the low-doped samples with $0.05 \leq x \leq 0.11$, they all show the similar behaviors. The deviation temperature T_D is also listed in Table 1. It also confirms the existence of the Griffiths phase. In the Griffiths phase region, the formation of the short-range FM phase is responsible for the deviated behavior of resistivity above T_C.

It should be noted that when x increases from 0.11 to 0.12, despite the fact that the increase in the doping level is very small, the change in magnetization under ZFC is large. According to the XRD, IR, and Raman spectra, the structure of the compounds does not change. Then, what is the reason of the remarkable change in magnetization curve? We know that in the hexa-coordination environment, the ionic radius of Ga^{3+} (0.62 Å) is smaller than that of Mn^{3+} (0.645 Å). Based on the model proposed by Alonso et al. [18], Ga doping will induce the hole localization. The charge of Ga ion is always +3 while the charge of Mn ion is a mixture of +3 and +4. Therefore holes cannot hop onto Ga ions, but Ga ions are attracted to them. Due to the difference between Mn^{3+} and Ga^{3+} ionic radius, there appears an additional electrostatic potential ε felt by a hole at Mn ions with only one neighboring Ga. With the increase in the Ga substitution, the probability of Mn ion surrounded with Ga^{3+} increases, so more holes will be localized. The hole localization suppresses the Mn–O–Mn DE interaction and

meanwhile enhances the systematic insulating property. When the doping level exceeds a critical point x_c, the metal–insulating transition disappears and the whole curve exhibits the insulating behavior. From Fig. 5, we can get that the critical point is close to 0.12, which is in agreement with the value ($x_c = 0.1$–0.2) deduced by Alonso et al. in the $La_{2/3}Ca_{1/3}Mn_{1-x}Ga_xO_3$ system [18]. In this system, with increasing Ga concentration, the interplay among the DE interaction, the effect of hole location, and the disorder caused by the Ga substitution takes the system from a long-range FM state to a cluster-spin-glass state.

It should be emphasized that, for $x = 0.12$ (shown in the inset of Fig. 4), with the decrease in temperature, the ZFC curve below T_C decreases firstly as one for $x = 0.15$, which indicates the character of cluster-spin glass and that there is no interaction between these separate clusters, and then decreases slowly and flatly below 50 K as one for $x = 0.11$, which indicates that the interaction between these separate clusters takes place and that the system forms a long-range FM order, exhibiting the Griffiths singularity.

In summary, for the parent and low-doping samples ($0 \leq x \leq 0.11$), $Nd_{0.7}Sr_{0.3}Mn_{1-x}Ga_xO_3$ system shows a long-range FM state below T_C and the Griffiths singularity above T_C. When x further exceeds 0.12, a transition from the FM metal to the CSG insulating state as a function of Ga doping takes places at low temperatures.

Acknowledgements

This work is supported by National Natural Science Foundation of China through Grant No. 10334090, No. 10504029, and the State Key Project of Fundamental Research, China, No. 001CB610604.

References

[1] E.L. Nagaev, Phys. Rep. 346 (2001) 387.
[2] E. Dagotto, T. Hotta, A. Moreo, Phys. Rep. 344 (2001) 1.
[3] Y. Tokura, Rep. Progr. Phys. 69 (2006) 797.
[4] A. Maignan, C. Martin, B. Raveau, Z. Phys. B: Condens. Matter 102 (1997) 19.
[5] K. Ghosh, S.B. Ogale, R. Ramesh, R.L. Greene, T. Venkatesan, K.M. Gapchup, Ravi Bathe, S.I. Patil, Phys. Rev. B 59 (1999) 533.
[6] Mark Rubinstein, D.J. Gillespie, John E. Snyder, Terry M. Tritt, Phys. Rev. B 56 (1997) 5412.
[7] A. Maignan, F. Damay, A. Barnabé, C. Martin, M. Hervieu, B. Raveau, Philos. Trans. R. Soc. London, Ser. B 356 (1998) 1635.
[8] Young Sun, Xiaojun Xu, Lei Zheng, Yuheng Zhang, Phys. Rev. B 60 (1999) 12317.
[9] M.B. Salamon, P. Lin, S.H. Chun, Phys. Rev. Lett. 88 (2002) 197203.
[10] J. Deisenhofer, D. Braak, H.-A. Krug von Nidda, J. Hemberger, R.M. Eremina, V.A. Ivanshin, A.M. Balbashov, G. Jug, A. Loidl, T. Kimura, Y. Tokura, Phys. Rev. Lett. 95 (2005) 257202.
[11] R.B. Griffiths, Phys. Rev. Lett. 23 (1969) 17.
[12] A.J. Bray, M.A. Moore, J. Phys. C 15 (1982) L765.
[13] A.J. Bray, Phys. Rev. Lett. 59 (1987) 586.
[14] L. Martín-Carrón, A. de Andrés, J. Alloys Compd. 323–324 (2001) 417–421.
[15] M.N. Iliev, M.V. Abrashev, H.G. Lee, V.N. Popov, Y.Y. Sun, C. Thomsen, R.L. Meng, C.W. Chu, Phys. Rev. B 57 (1998) 2872.
[16] J.A. Mydosh, Spin Glass: An Experimental Introduction, Taylor and Francis, London, 1993.
[17] A.H. Castro Neto, G. Castilla, B.A. Jones, Phys. Rev. Lett. 81 (1998) 3531.
[18] J.L. Alonso, L.A. Fernandez, F. Guinea, V. Laliena, V. Martin-Mayor, Phys. Rev. B 66 (2002) 104430.